NASA TECHNICAL MEMORANDUM

NASA TM X-2398

NASA TM X-2398

EXPERIMENTAL TECHNIQUES FOR EVALUATING STEADY-STATE JET ENGINE PERFORMANCE IN AN ALTITUDE FACILITY

by John M. Smith, Chi Y. Young, and Robert J. Antl

Lewis Research Center

Cleveland, Ohio 44135

NATIONAL AERONAUTICS AND SPACE ADMINISTRATION • WASHINGTON, D. C. • NOVEMBER 1971

1. Report No.	2 Government Accession No.	3 Recipient's Catalog No
NASA TM X-2398		

4. Title and Subtitle	5 Report Date
EXPERIMENTAL TECHNIQUES FOR EVALUATING STEADY-STATE JET ENGINE PERFORMANCE IN AN ALTITUDE FACILITY	November 1971
	6. Performing Organization Code

7. Author(s)	8 Performing Organization Report No.
by John M. Smith, Chi Y. Young, and Robert J. Antl	E-6392
	10 Work Unit No
	720-03

9. Performing Organization Name and Address	11 Contract or Grant No
Lewis Research Center National Aeronautics and Space Administration Cleveland, Ohio 44135	

12. Sponsoring Agency Name and Address	13 Type of Report and Period Covered
National Aeronautics and Space Administration Washington, D. C. 20546	Technical Memorandum
	14 Sponsoring Agency Code

15. Supplementary Notes

16 Abstract

Jet engine calibration tests were conducted in an altitude facility at the NASA Lewis Research Center using a contoured bellmouth inlet duct, four fixed-area water-cooled exhaust nozzles, and an accurately calibrated thrust measuring system. Accurate determination of the airflow measuring station flow coefficient, the flow and thrust coefficients of the exhaust nozzles, and the experimental and theoretical terms in the nozzle gross thrust equation were some of the objectives of the tests. A primary objective was to develop a technique to determine gross thrust for the turbojet engine used in this test that could also be used for future engine and nozzle evaluation tests. The probable error in airflow measurement was found to be approximately 0.6 percent at the bellmouth throat design Mach number of 0.6. The probable error in nozzle gross thrust measurement was approximated 0.6 percent at the load cell full-scale reading.

17. Key Words (Suggested by Author(s))	18. Distribution Statement
Experimental techniques; Turbojet engine; Gross thrust; Airflow calibration; Altitude facility; Convergent-divergent fixed area nozzles	Unclassified - unlimited

19. Security Classif. (of this report)	20 Security Classif (of this page)	21 No of Pages	22 Price*
Unclassified	Unclassified	39	$3.00

* For sale by the National Technical Information Service, Springfield, Virginia 22151

EXPERIMENTAL TECHNIQUES FOR EVALUATING STEADY-STATE JET ENGINE PERFORMANCE IN AN ALTITUDE FACILITY

by John M. Smith, Chi Y. Young, and Robert J. Antl

Lewis Research Center

SUMMARY

Airflow and thrust calibration tests were conducted on a J85 afterburning turbojet engine in an altitude facility of the NASA Lewis Research Center using a contoured bellmouth inlet duct, four fixed-area water-cooled exhaust nozzles, and an accurately calibrated thrust system.

Accuracy in these calibrations was of prime concern in this program. The probable experimental error in airflow measurement was 0.6 percent near the bellmouth throat design Mach number of 0.6. This probable error was based on individual and cumulative errors of instrumentation. The probable error in gross thrust measurement was approximately 0.6 percent at the load cell full-scale reading. This was based on instrumentation, data systems, and thrust load cell errors.

A simplified method for calculating airflow rate is presented and validated by a more rigorous method when the inlet airflow conditions are favorable.

The isentropic thrust coefficients and the gross thrust coefficients for the exhaust nozzles were experimentally determined with and without an engine in place. A J85 turbojet engine was used for the hot runs.

The values of the isentropic thrust coefficients from hot-gas data were on the average within ±0.59 percent of the cold-flow values using the cold-flow data as a base line.

INTRODUCTION

Flight flying test bed and wind-tunnel evaluation of supersonic exhaust nozzles operating in the transonic flight regime are currently underway at Lewis. In order to determine nozzle characteristics, the nozzle inlet total pressure, temperature, and gas flow rate must be known. Obtaining these measurements is sometimes difficult as in the case

of the flying test bed. Therefore, these variables must be determined accurately in ground-test facilities.

Engine thrust is one of the prime design variables and accurate calibrations and measurements are needed to determine the gross thrust and nozzle thrust coefficients. A prime requirement is the design of a thrust measuring system to evaluate gross thrust within the required accuracy.

Airflow is also a prime engine variable. An airflow measuring station is invariably incorporated in any engine test setup. The flow calibration of the airflow measuring station can be determined using temperature and pressure measurements.

Flow conditions at the inlet of the exhaust nozzle must be known in order to determine the nozzle coefficients. The use of fixed-area water-cooled nozzles provides a means of accurately determining nozzle throat area by minimizing thermal expansion. The technique of using water-cooled nozzles is reported on in reference 1. Exhaust nozzle thrust coefficients for both hot-gas and cold-flow runs have been calculated and compared using the cold flow data as a base line. This comparison is needed to show that the thrust measuring system designed for these tests could evaluate gross thrust within the desired accuracy for a turbojet engine, and that the thrust system could also be used for other engine and nozzle evaluation tests. Several nozzle evaluation test results are reported in references 2 to 4.

Hot gas was provided by a J85 turbojet engine with an afterburner with exhaust gas temperatures up to 1944 K (3500° R).

All tests were conducted in the NASA Lewis Research Center Propulsion Systems Laboratory.

APPARATUS

Figure 1 shows a schematic diagram of the contoured inlet air bellmouth that was used for the tests. The inlet of the bellmouth and a portion of the length was based on an ASME design. The remainder of the length was designed for sinusoidal acceleration. The inlet airflow measuring station (station 1) was designed for a throat Mach number of 0.6.

Figure 2(a) shows a schematic drawing of the test installation of the duct used for the cold-flow tests. The dimensions of the straight cold-flow duct were approximately the same as a J85 turbojet engine. It was 40.64 centimeters (16 in.) at the inside diameter and 238.76 centimeters (94 in.) long. A screen was installed in the duct for use with any nozzle that had a throat diameter larger than that of the bellmouth straight section. This was to insure that the nozzle would choke instead of the bellmouth straight section.

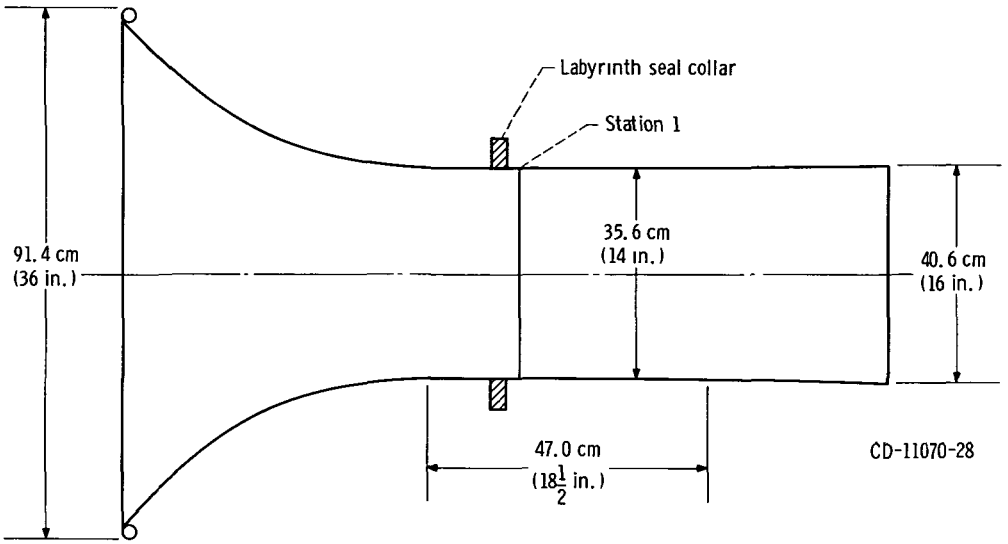

Figure 1. - Inlet air bellmouth.

After the cold-flow tests, a J85 turbojet engine was installed as a gas generator for the hot-gas tests. Figure 2(b) shows a schematic drawing of the test installation of a J85 engine for the hot-gas tests. The engine was approximately 50.8 centimeters (20 in.) at the outside diameter and 276.86 centimeters (109 in.) in length including the afterburner. The engine has an eight-stage axial-flow compressor coupled directly to a two-stage turbine. The engine also has an annular primary combustion system, variable inlet guide vanes, controlled compressor interstage bleed, afterburner, and variable-area exhaust nozzle. The variable-area nozzle was replaced by the fixed-area water-cooled nozzles used for these calibration tests and those reported in reference 1.

Figure 3(a) is a photograph showing a water-cooled nozzle with cooling lines attached, fastened to the afterburner of the J85 engine. A schematic of the interior contours of these nozzles is shown in figure 3(b). The nozzles were convergent-divergent types with a contoured convergent section and a throat radius of curvature equal to the throat diameter. The divergent portion was a 15° half-angle cone with an expansion area ratio of approximately 1.3. The throat areas were 694, 843, 1073, and 1186 square centimeters (107.5, 130.7, 166.3, and 183.8 $in.^2$), respectively.

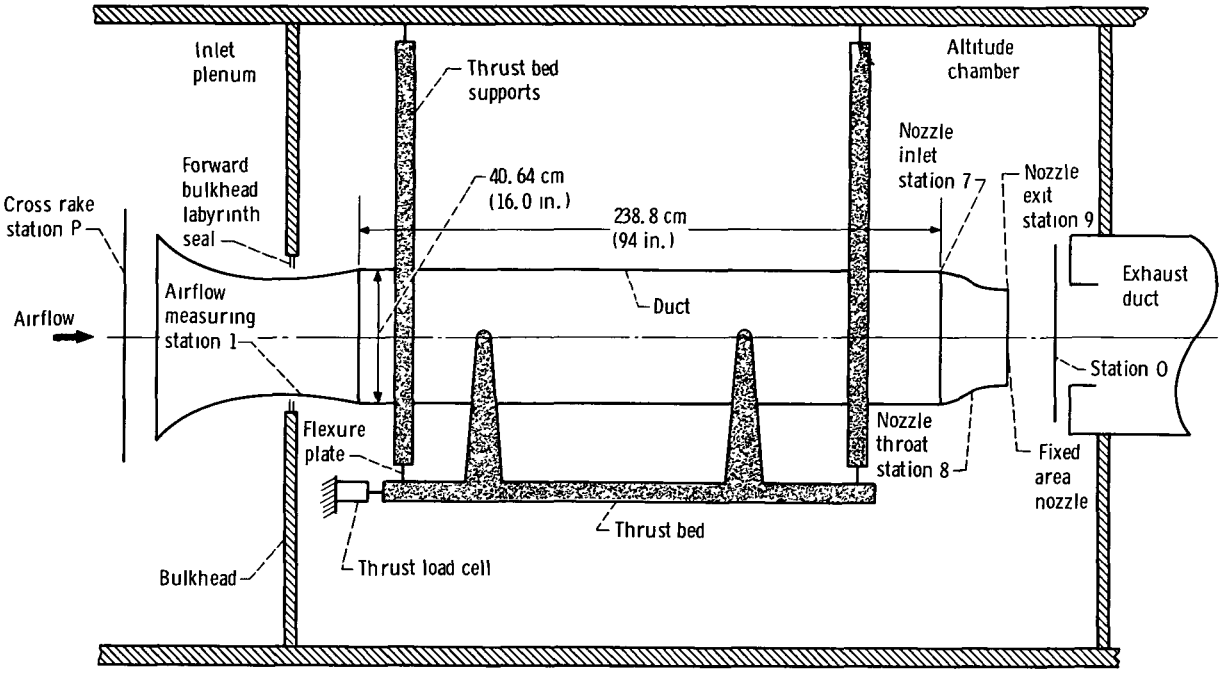

(a) Test installation of duct for cold-flow tests.

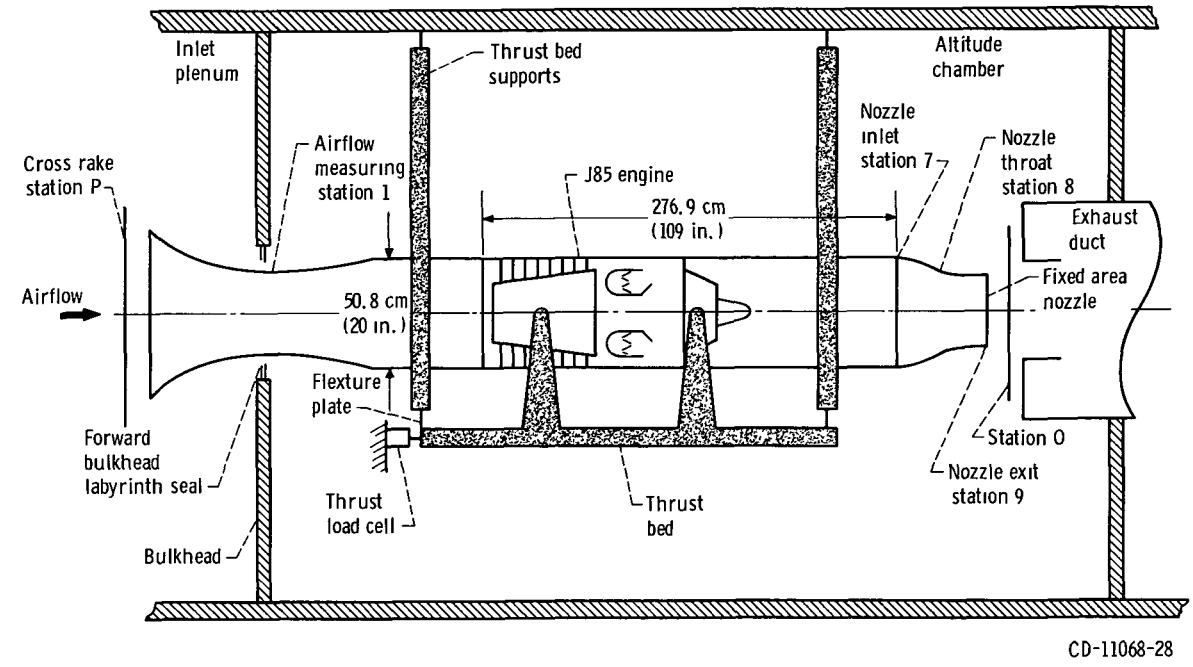

(b) Test installation of J-85 turbojet engine for hot-gas test.

Figure 2. - Test installation for cold-flow and hot-gas tests.

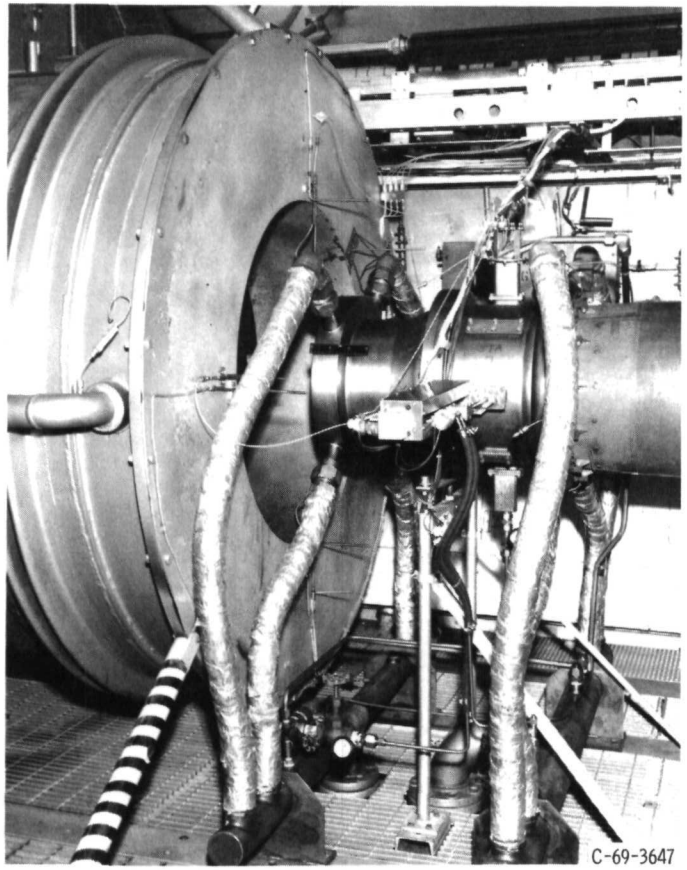

(a) Test installation of water-cooled nozzle.

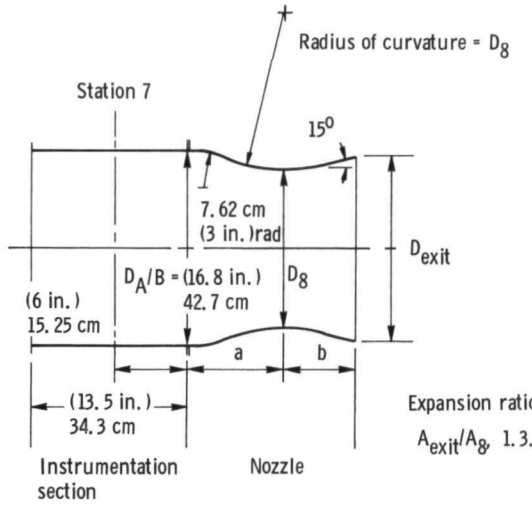

Nozzle throat area, A_8		Nozzle throat diameter, D_8		Nozzle exit diameter, D_{exit}		Nozzle exit area, A_{exit}		Nozzle inlet to throat, a		Nozzle throat to exit, b	
cm^2	$in.^2$	cm	in.	cm	in.	cm^2	$in.^2$	cm	in.	cm	in.
694	107.5	29.7	11.7	33.9	13.35	903	140	23.25	9.15	11.75	4.63
843	130.7	32.8	12.9	37.4	14.7	1095	169.7	21.62	8.51	12.86	5.06
1073	166.3	37.0	14.55	42.2	16.6	1396	216.4	17.94	7.06	14.58	5.74
1186	183.8	38.9	15.3	44.2	17.4	1534	237.8	15.41	6.06	15.07	5.93

(b) Water-cooled nozzle description and internal contour dimensions.

Figure 3. - Water-cooled nozzles.

FACILITY

The test program was conducted in the Propulsion Systems Laboratory Altitude Chamber at the NASA Lewis Research Center. In this facility, altitude from sea level to 24 000 meters (80 000 ft) can be simulated with airflow rates from 218 to 23 kilograms per second (480 to 50 lb/sec), respectively. Pressure ratio can also be varied over a wide range. In this test program the inlet to exhaust pressure ratio covered a range from 1.2:1 to 32:1. The inlet air bellmouth passed through a labyrinth seal in the chamber forward bulkhead and was directly connected to either the straight duct or the J85 engine. This system was mounted on a thrust measuring stand as shown in figure 2.

INSTRUMENTATION

Instrumentation was provided to measure the necessary parameters to calibrate the airflow measuring station, evaluate the flow and thrust coefficients of the nozzles, and evaluate the experimental and theoretical terms in the thrust equation. Measurements were located in the inlet plenum P the airflow measuring station (1), the nozzle inlet (7), and the altitude chamber (0) as shown in figure 2. Details of the locations of the pressure and temperature instrumentation at each station and on the bellmouth surface are shown in figure 4 as viewed from upstream. Other pressure probes located at the back of the bellmouth slightly ahead of the labyrinth seal and in the altitude chamber are not shown.

The data were recorded on the Lewis central automatic digital data encoder (CADDE). Temperatures were recorded as voltage outputs on the automatic voltage digitizer (AVD) system, and pressures were recorded on the digital automatic multiple pressure recording system (DAMPR). The data were then processed in a digital computer. A detailed description of the CADDE system is given in reference 5.

The total pressure probes used on the pressure rakes were single tubes with a 40° internal chamber. Information on the design of these probes can be found in reference 6. Total temperatures at stations 1 and 7 were corrected using recovery factors that were function of Mach number. These recovery factors were obtained from data in reference 7.

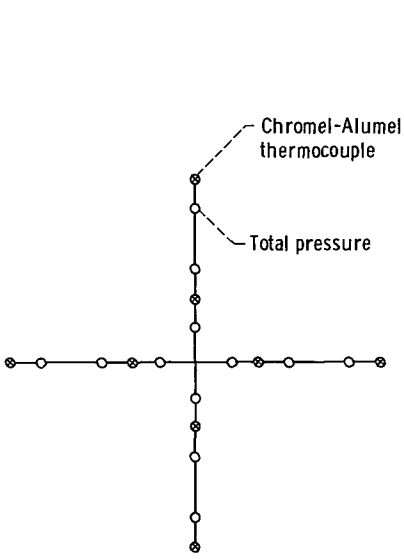

(a) Inlet plenum (sta. P) cross-rake, 30.48 cm (12 in.) upstream of bellmouth.

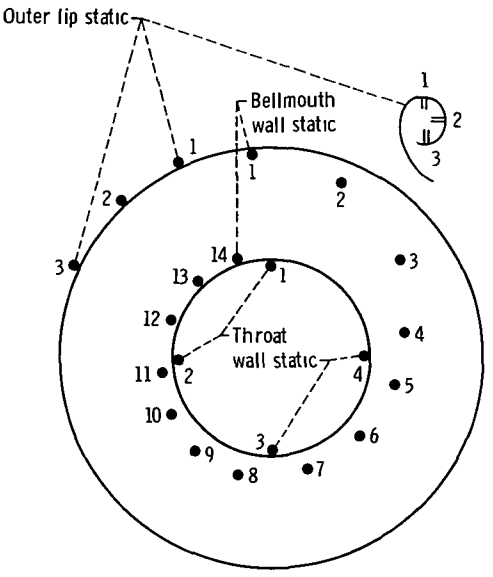

(b) Bellmouth static pressure.

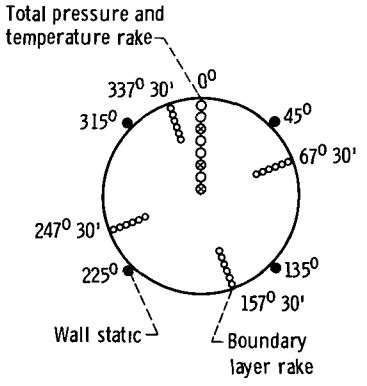

(c) Station 1 - downstream end of bellmouth throat straight section.

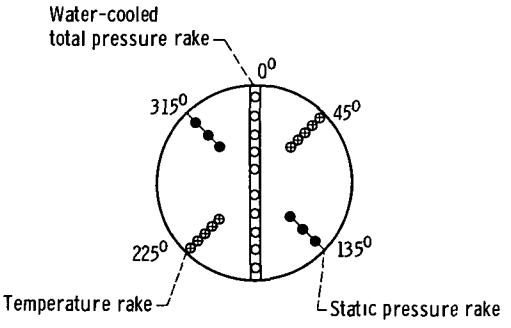

(d) Nozzle inlet (station 7).

CD-11069-28

Figure 4. - Bellmouth and duct instrumentation stations as viewed from upstream.

THRUST SYSTEM

One of the primary purposes of these tests was to determine the accuracy of the thrust measuring system in evaluating gross thrust for the turbojet engine and whether this thrust system could be used in other engine and nozzle tests.

As can be seen in figure 2, the test bed supporting either the straight duct or the J85 engine was suspended by flexure plates from facility supports.

A Baldwin Lima Hamilton double bridge load cell with a 22 240-N (5000-lbf) range was used to measure thrust. It was water cooled to minimize drift from heating in the test cell. The load cell was calibrated with a Morehouse proving ring and the combined nonlinearity and hysteresis was within ±0.1 percent of the load cell full-scale reading.

PROCEDURE

A series of tests were made to determine the flow coefficient of the airflow measuring station, the flow and thrust coefficients of the four fixed-area nozzles, and experimental terms in the gross thrust equation.

The inlet (plenum) and altitude chamber pressures were varied to cover a wide range of pressure ratio (P_p/P_0), while the inlet air temperature was set about 311 K (560° R) for all tests. (All symbols are defined in appendix A.)

Airflow Calibration

The flow rate calibration tests consist of two parts: one on the airflow measuring station, and the other on the four fixed-area nozzles. The inlet pressure P_p was varied from 34.5 to 144.8 kilonewtons per square meter absolute (5 to 21 psia), and, at each P_p, the altitude chamber pressure was varied to give a range of P_p/P_0 from 1.2 to 30 as shown in table I.

TABLE I. - AIRFLOW CALIBRATION

TEST PRESSURES (NOMINAL)

Plenum pressure		Pressure ratio, P_p/P_0 to P_7/P_0
kN/m^2	psia	
34.5	5.0	1.2 to 15.0
101.4	14.7	1.2 to 24.0
124.1	18.0	1.2 to 27
144.8	21.0	1.5 to 30

Airflow Measuring Station Calibration

The accuracy of engine or component tests rests on the ability to determine accurately the airflow passing through the test article. One frequently used method is based on the continuity equation. For a compressible but perfect gas, the continuity equation can be expressed as

$$W = AP\left[\frac{2g\gamma}{RT(\gamma - 1)}\right]^{1/2}\left(\frac{p}{P}\right)^{1/\gamma}\left[1 - \left(\frac{p}{P}\right)^{(\gamma-1)/\gamma}\right]^{1/2} \tag{1}$$

At the throat of the bellmouth (station 1), static and total pressures are recorded by probes located as shown in figure 4(c). There is one rake with five total pressure probes across the mainflow area of the throat, and there are four rakes each with six total pressure probes for boundary-layer measurements plus four wall static pressure taps.

An average total pressure $\overline{P}_1$ at station 1 was obtained from the relation

$$\overline{P}_1 = \frac{1}{A_1}\int P_1 \, dA \tag{2}$$

The actual procedure in obtaining $\overline{P}_1$ was as follows: $\overline{P}_1(1)$ was evaluated using equation (2) with values of the five main flow area probes plus one set of values from one boundary layer rake. This calculation was repeated for each of the remaining three boundary-layer rakes. Then, $\overline{P}_1$ was equal to the average of these four values

$$\overline{\overline{P}_1} = \frac{1}{4}\left[\overline{P}_1(1) + \overline{P}_1(2) + \overline{P}_1(3) + \overline{P}_1(4)\right] \tag{3}$$

Figure 5 shows a typical plot of total pressure as a function of area. The last points on the curved portion are the boundary layer rake values.

Using $\overline{P}_1$ as the total pressure in equation (1), the actual airflow W_1, at the bellmouth throat was calculated. Then using the measured total pressure $P_{1,id}$ (not including the boundary layer values) at station 1 and equation (1), an ideal airflow, $W_{1,id}$ was calculated. An ideal airflow was also calculated using the average total pressure P_p in the plenum and equation (1).

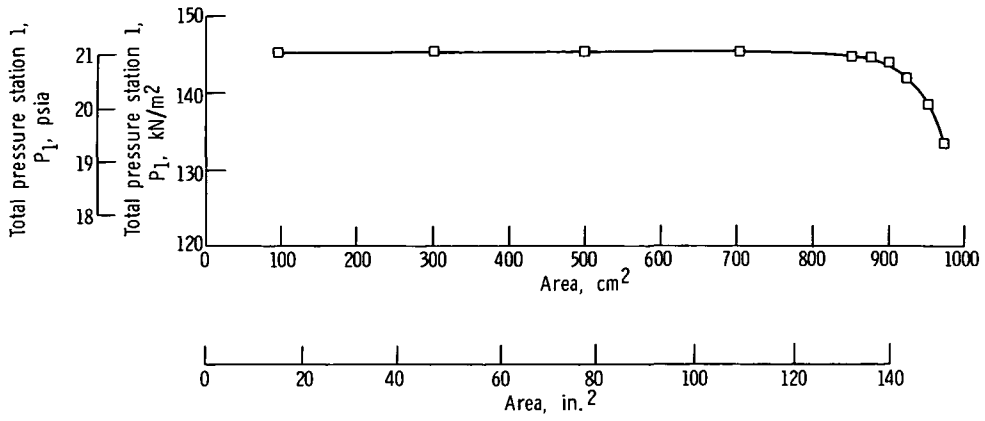

Figure 5. - Station 1 total pressure including boundary-layer rake total pressures as function of area.

In order to compare values of air flow under different inlet and exit conditions, a dimensionless flow parameter is used. It is known commonly as the discharge coefficient C_D. It is defined as

$$C_{D,bm} = \frac{\text{Calculated actual air flow}}{\text{Calculated ideal air flow}} = \frac{W_1}{W_{1,id}} \tag{4}$$

Values of the discharge coefficient were calculated using ideal flow based on total pressure $P_{1,id}$ at station 1 as shown in figure 6(a). Values of the discharge coefficient

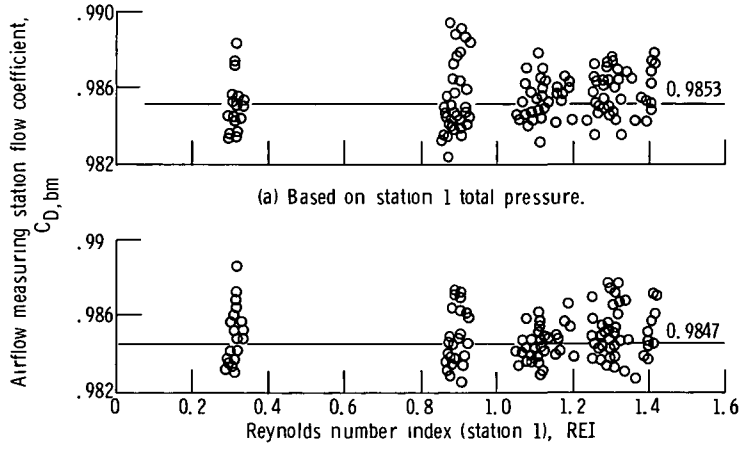

Figure 6. - Airflow measuring station flow coefficient as function of Reynolds number index for cold-flow data

TABLE II. - FLOW RATE CALCULATION USING METHOD OF ANNULUS AREA SUMMATION

Number of annulus, K	Total pressure in annulus, P_K		Airflow in each annulus, W_K	
	kN/m^2	psia	kg/sec	lb/sec
1	131.828	19.120	1.0458	2.3056
2	↓	↓	↓	↓
3				
4				
5				
6				
7				
8				
9				
10				
11				
12				
13				
14	↓	↓	↓	↓
15	131.814	19.118	1.0454	2.3047
16	131.800	19.116	1.0450	2.3038
17	131.655	19.095	1.0407	2.2943
18	131.276	19.040	1.0293	2.2693
19	129.966	18.850	.9891	2.1807
20	124.519	18.060	.7999	1.7634

Annulus area, $\frac{1}{20}$ (993.16 cm) = (49.658 cm^2) (or 7.697 $in.^2$)

Static pressure station 1, p = 114.33 kN/m^2 (or 16.5822 psi)

Inlet air temperature, 310.69 K (or 559.24° R)

Airflow in each annulus, $$W_K = \left[\frac{2g\gamma}{RT(\gamma - 1)}\right]^{1/2} \left(\frac{p}{P_K}\right)^{1/\gamma} \left[1 - \left(\frac{p}{P_K}\right)^{(\gamma-1)/\gamma}\right]^{1/2} \Delta A_K$$

Total airflow station 1, $$W_1 = \sum_{k=1}^{20} W_K = 20.59 \text{ kg/sec (or 45.395 lb/sec)}$$

TABLE III. - COMPARISON OF BELLMOUTH FLOW COEFFICIENTS

Nozzle throat area, A_8		Bellmouth throat static pressure, p_1		Bellmouth flow coefficient, $C_{D,bm}$	
cm^2	$in.^2$	kN/m^2	psia	Simplified method	Summation method
694	107.5	114.33	16.58	0.98662	0.98433
694	107.5	108.11	15.68	.98406	.98785
843	130.7	113.54	16.47	.98648	.98878
843	130.7	58.34	8.89	.98331	.98269
1073	166.3	100.92	14.64	.98420	.98506
1073	166.3	80.66	11.70	.98598	.98451
1186	183.8	74.95	10.87	.98445	.98706
1186	183.8	93.76	13.60	.98577	.98888
Average of eight headings				0.98511	0.98615

were also calculated using values of plenum total pressure P_p for ideal flow as shown in figure 6(b).

In an effort to check the accuracy of the actual airflow calculation using equation (1), an actual airflow was calculated using the normal method of summation of annulus area. The flow area at station 1 was divided into 20 equal annulus areas. The air flow was calculated for each of these areas and summed to give the air flow for the whole duct. The results are shown in table II. A comparison of the results obtained using the two different methods is shown in table III.

Exhaust Nozzle Calibration

An accurate calibration of air flow through the exhaust nozzle is required in many engine programs.

The procedure for determining the discharge coefficients for the four fixed-area nozzles is essentially the same as that for the inlet bellmouth. The actual air flow at the throat of the exhaust nozzle is equal to that calculated for the bellmouth if there is no leakage. Therefore, $W_8 = W_1$.

Using values measured at station 7 for total pressure and temperature and insuring that the exhaust nozzle is always choked, the ideal air flow at the nozzle throat can be calculated using the following equation:

$$W_{8,id} = \frac{A_8 P_{7,id}}{RT_7}\left(\frac{2}{\gamma+1}\right)^{1/\gamma-1}\left[2gRT_7\frac{\gamma}{\gamma-1}\left(1-\frac{2}{\gamma+1}\right)\right]^{1/2} \quad (5)$$

The exhaust nozzle discharge coefficient is therefore defined as

$$C_{D,n} = \frac{W_1}{W_{8,id}} \quad (6)$$

Thrust Equation Evaluation

One of the important engine performance parameters is the gross thrust. In the engine test facility, the load cell in the test stand records overall thrust exerted on it by the entire system. The overall thrust hereafter called F_m, the measured thrust includes, algebraically, (1) the gross thrust, (2) the pressure forces acting on the air inlet device, (3) the forces acting on the bulkhead seal due to pressure differential, and (4) the other miscellaneous facility system forces and restraints such as airflow leakage, structure joint friction, connecting piping, electrical lines, load cell hysteresis, and so forth. With proper facility design all the miscellaneous forces in item (4) can be made negligibly small, and are accounted for by a static calibration of the thrust measuring system.

The measured thrust of the test system can be defined by the equation

$$F_m = \left[(mv)_9 + p_9A_9 - P_0A_9\right] - \left[(mv)_{in} + p_{in}A_{in} - P_pA_{in}\right] - \left[A_s(P_p - P_0) + F_{fr,s} + F_d\right] \quad (7)$$

Since the gross thrust is defined as

$$F_g = \left[(mv)_9 + p_9A_9 - P_0A_9\right] \quad (8)$$

and letting

$$FIN = \left[(mv)_{in} + p_{in}A_{in} - P_pA_{in}\right] \quad (9)$$

then

$$F_g = F_m + FIN + \left[A_s(P_p - P_0) + F_{fr,s} + F_d\right] \tag{10}$$

Figure 7 shows the location and direction of these forces for the cold flow tests. A mechanical preload was used to insure a positive loading on the load cell at all times.

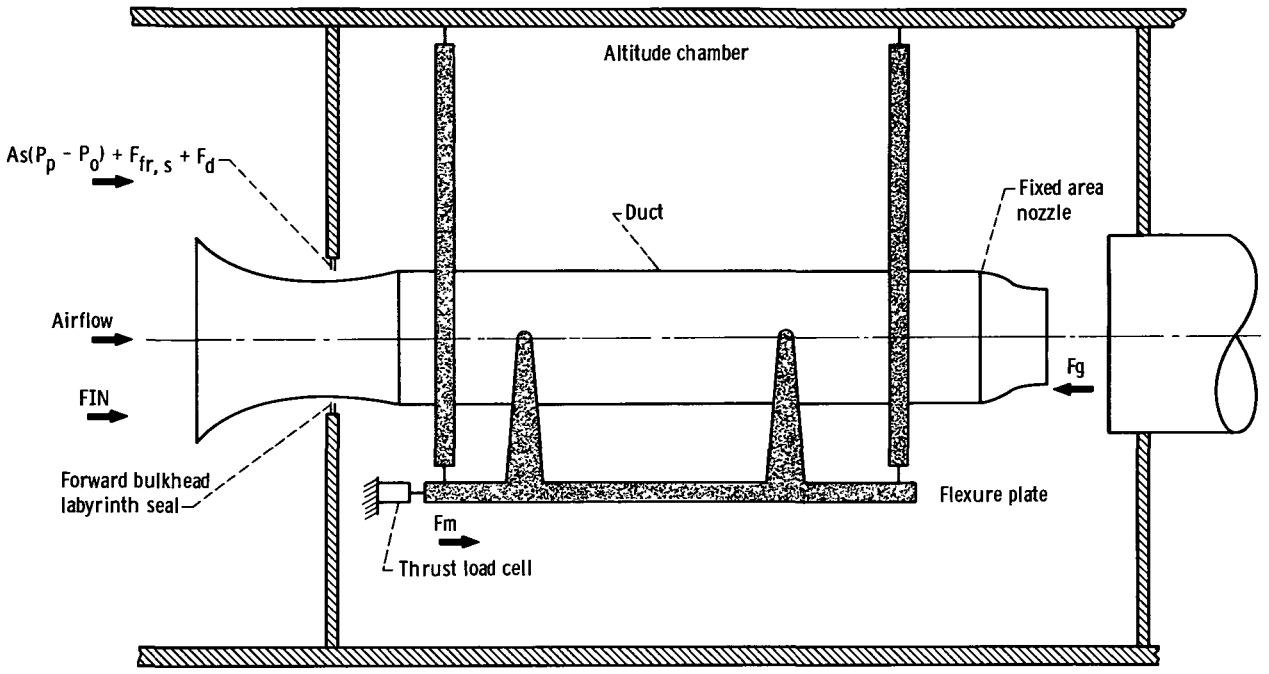

Figure 7. - Thrust system showing location and direction of thrust terms used in gross thrust equation for cold-flow tests.

TABLE IV. - THRUST CALIBRATION TEST

PRESSURES (NOMINAL)

Plenum pressure		Pressure differential, $P_p - P_0$	
kN/m^2	psia	kN/m^2	psi
34.5	5.0	6.9 to 31	1.0 to 4.5
101.4	14.7	13.8 to 96.5	2.0 to 14
124.1	18.0	13.8 to 120	2.0 to 17.5
144.8	21.0	17.2 to 141	2.5 to 20.5

The term FIN and the bracketed term in equation (10) must be determined in order to properly evaluate the gross thrust of the test article.

The thrust equation evaluation program tests covered a range of inlet pressure P_p from 34.5 to 144.8 kN/m^2 (5 to 21 psia), and of altitude chamber pressure P_0 such that $(P_p - P_0)$ varied from 6.9 to 138.0 kN/m^2 (1 to 20 psi) as shown in table IV.

Bellmouth Pressure Forces

The FIN term in the right side of equation (10) represents the momentum and the forces exerted on the bellmouth inlet due to the varying static pressure differential acting on the large and varying area curved surface.

A theoretical determination of the combined bellmouth inlet pressure force term, $FIN = (mv)_{in} + p_{in}A_{in} - P_pA_{in}$ was made in terms of the corrected airflow rate at the bellmouth inlet. Therefore,

$$\frac{FIN}{P_p} = A_{in}(Q - 1) \tag{11}$$

where

$$Q = Gc^2 \frac{R}{g}\left(\frac{p_{in}}{P_{in}}\right)^{-1/\gamma} + \frac{p_{in}}{P_{in}} = \gamma M_{in}^2 \frac{p_{in}}{P_{in}} + \frac{p_{in}}{P_{in}} \tag{12}$$

The parameter Q calculated as a function of Gc and p_{in}/P_{in} is given in reference 8. Thus, FIN can be calculated once the flow rates are known.

Forces on the bellmouth seal and drag forces. - The second bracketed term in equation (10) is composed of forces due to the difference in inlet plenum pressure and altitude chamber pressure and the restraining or frictional force produced by air flowing through the seal gap. There are also base drag forces included in this second term. The combined seal force plus drag force can be determined experimentally. To do this, the duct was blanked downstream of the airflow measuring station (station 1), and pressures in the plenum and altitude chamber were set as shown in table IV. Since there is no mass flow through the duct, $(mv)_9 = 0$ and $p_9 = p_0 = P_0$. Therefore, $F_g = 0$.

Furthermore, $(mv)_{in} = 0$ and $p_{in} = P_p$. Equation (4) is reduced to

$$F_m = -\left[A_s(P_p - P_0) + F_{fr,s} + F_d\right] \tag{13}$$

That is the measured thrust in this test setup consists of the combined $A_s\Delta_P$ and friction seal force plus drag forces. After FIN and the bracketed term are determined, the gross thrust can be determined.

Gross thrust coefficient. - The ideal thrust equation is as follows:

$$F_{id} = C_{F,id} P_7 A_8 C_{D,n} \tag{14}$$

where

$$C_{F,id} = \gamma \left\{ \frac{2}{\gamma - 1} \left(\frac{2}{\gamma + 1} \right)^{\gamma+1/\gamma-1} \left[1 - \left(\frac{p_9}{P_9} \right)^{\gamma-1/\gamma} \right] \right\}^{1/2} + \frac{p_9 - P_0}{P_7} \frac{A_9}{A_8} \tag{15}$$

For any given nozzle and fixed inlet conditions of γ, p_9, P_7, A_8, A_9, and P_9

$$C_{F,id} = (\text{Constant}) - \frac{p_0}{P_7} \frac{A_9}{A_8} \tag{16}$$

Thus the ideal slope when plotted as a function of P_0/P_7 is a straight line with a slope equal to the nozzle area ratio A_9/A_8.

We can also define a similar coefficient with the expression

$$F_g = C_F P_7 A_8 C_{D,n} \tag{17}$$

or

$$C_F = \frac{F_g}{P_7 A_8 C_{D,n}} \tag{18}$$

where C_F is the actual gross thrust coefficient.

When the flow is expanded isentropically in the diverging section of the nozzle, the nozzle exit static pressure is fixed by the inlet total pressure and the nozzle area ratio. If the altitude chamber pressure P_0 is equal to or less than the nozzle exit pressure p_9, the nozzle will flow full. As P_0 increases above this value, flow separation will occur. When separation occurs the flow is apt to be more erratic and there is a loss

connected with the associated shock waves. The variation of C_F against P_0/p_7 should then reflect this and will no longer be a straight line. We have used this feature as an indication of nozzle flow separation, although direct observation was not made to confirm it.

Airflow Error Analysis

Efforts were made to determine the resulting probable error in airflow computation due to various instrumentation errors. In general, the probable error is about ±0.4 percent at the bellmouth throat design Mach number of 0.6. Details are given in appendix B.

Gross Thrust Error Analysis

Similarly an error analysis was made on the measurement of gross thrust. Calculations indicated that the probable error was about ±0.3 percent at the load cell full-scale reading. Details are given in appendix C.

Hot-Gas Flow Tests

After the cold-flow calibration test runs were completed, a J85 turbojet engine was installed in the test stand. Hot-gas test runs were made with similar plenum and altitude chamber pressure settings up to exhaust gas temperatures of 1944 K (3500° R). Isentropic thrust coefficients and gross thrust coefficients were calculated for the exhaust nozzles.

RESULTS

The results are presented in three parts: first, the results of the cold-flow calibration of the airflow measuring station, and the thrust and flow coefficients of the four fixed-area nozzles; second, the results of the hot-gas tests with a J85 engine which determined gross thrust and thrust coefficients for the four nozzles; and, third, a comparison of the isentropic thrust coefficients for the hot-gas and cold-flow tests using the cold-flow data as a base line.

Cold-Flow Tests

Flow measuring station (bellmouth inlet) calibration. - The average total pressure at station 1, $\overline{P}_1$ was evaluated by area integration of the recorded total pressure. A typical plot of P_1 against flow area A_1 is shown in figure 5.

The actual flow at the airflow measuring station was calculated using $\overline{P}_1$ and the continuity equation. The actual airflow was also calculated by the method of summation of areas to check the method using the continuity equation and a single value of the total pressure. Table III compares several flow coefficients calculated using the airflow from the two methods. Agreement between them was generally within ±0.2 percent.

Airflow measuring station flow coefficients. - The bellmouth flow coefficients were computed by dividing the calculated actual airflow using $\overline{P}_1$ and p_1 by the ideal flow rate, calculated using the free-stream total pressure without B/L probes at station 1, $P_{1,id}$ and p_1. The results are presented in figure 6(a).

The bellmouth flow coefficients were also calculated by dividing the actual airflow by the ideal flow rate calculated using the average plenum total pressure P_p and p_1. The results are presented in figure 6(b).

Comparison of the flow coefficients obtained by the two methods showed that agreement was excellent. With either method the scattering of data points were all within a band of about ±0.4 percent. The difference between the average values from the two methods is less than 0.07 percent.

It was therefore concluded that using the plenum pressure for the calculation of the ideal air flow would be quite accurate. Thus, the total pressure rake at station 1 could be eliminated for the hot-gas tests. This would provide a smoother airflow into the engine inlet as long as there was uniform bellmouth inlet conditions.

Exhaust nozzle flow calibrations. - The four fixed-area water-cooled exhaust nozzles are all convergent-divergent with an exit to throat area ratio (A_9/A_8) of about 1.3. The dimensions are given in figure 3(b). These four nozzles were also used in the test program reported in reference 1. The pressure settings in the calibration runs are given in table I.

The total air flow rate of station 8 was calculated with equation (5) using average total pressure at station 7, $P_{7,id}$. Figure 8 is a plot of typical recorded total pressures at nozzle inlet against the radii where the probes were located. These total pressures were integrated with respect to flow area and averaged to give $P_{7,id}$. In calibration runs, the actual air flow rate through the nozzle is assumed to be the same as the actual flow rate at station 1, that is $W_8 = W_1$.

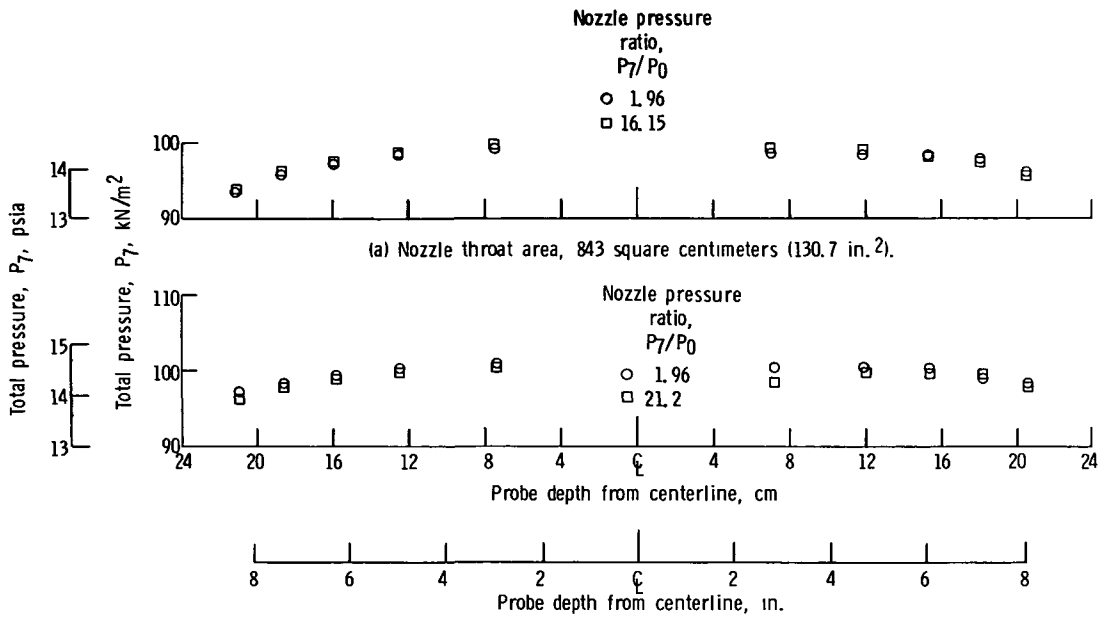

Figure 8. - Typical nozzle inlet (station 7) total pressure profiles for cold-flow data. Plenum total pressure, atmospheric.

The exhaust nozzle discharge coefficients were computed using the definition that

$$C_{D,n} = \frac{W_1}{W_{8,id}} \tag{19}$$

These coefficients are presented in figure 9. The scattering of data points are within a ±0.5 percent band except for the nozzle with a throat area of 694 square centimeters (107.5 in.^{2}) which is about ±0.7 percent. The average value of the discharge coefficient for each of the four nozzles varies from 0.9946 to 1.0025. Although it is quite common to have nozzle discharge coefficients greater than 1 for several valid reasons as discussed in reference 9, while flowing hot gases, no clear cut reason can be given for these values greater than 1 determined using air at room temperature. However, data system accuracy and installation effects are the probable reasons for obtaining these values.

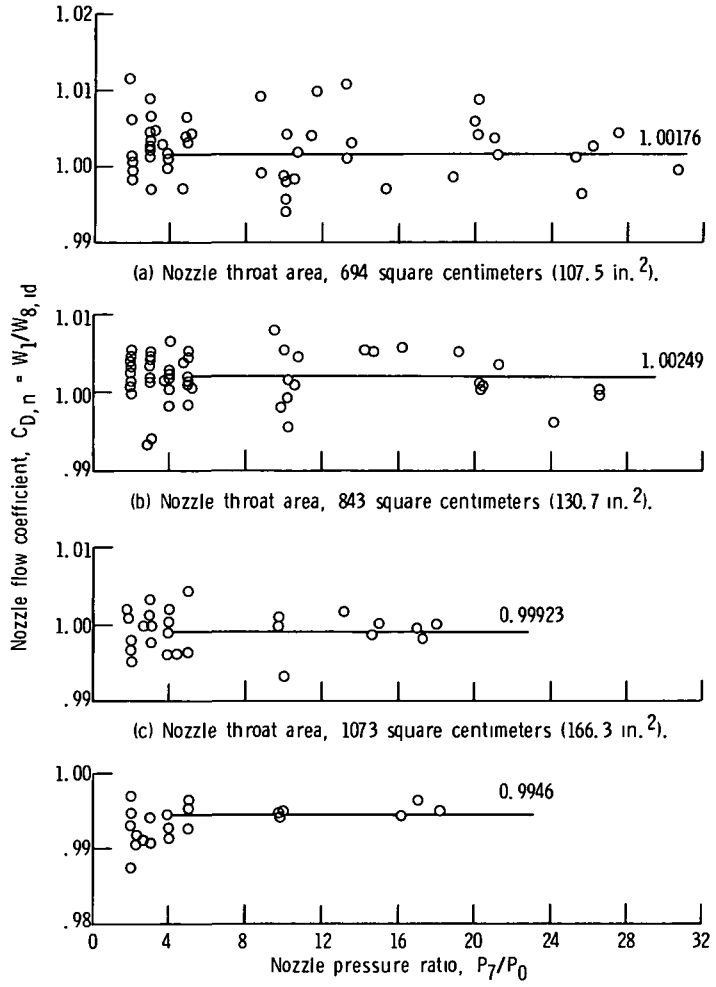

Figure 9. - Nozzle flow coefficient as function of nozzle pressure ratio for cold flow data.

Thrust Measurements

The exhaust nozzle thrust calibration and evaluation tests were conducted with the nominal pressure settings shown in table IV. The gross thrust is defined by equation (10).

Combined seal force term plus base drag force. - Physically the pressure probes for P_p were located in the plenum slightly ahead of the labyrinth seal, and probes for P_0 were in the altitude chamber at a location roughly where the throat of the exhaust nozzle would have been as shown in figure 2(a).

A typical result is shown in figure 10 where the experimentally determined seal force plus drag force is plotted against $(P_p - P_0)$. It is seen that the data follow an al-

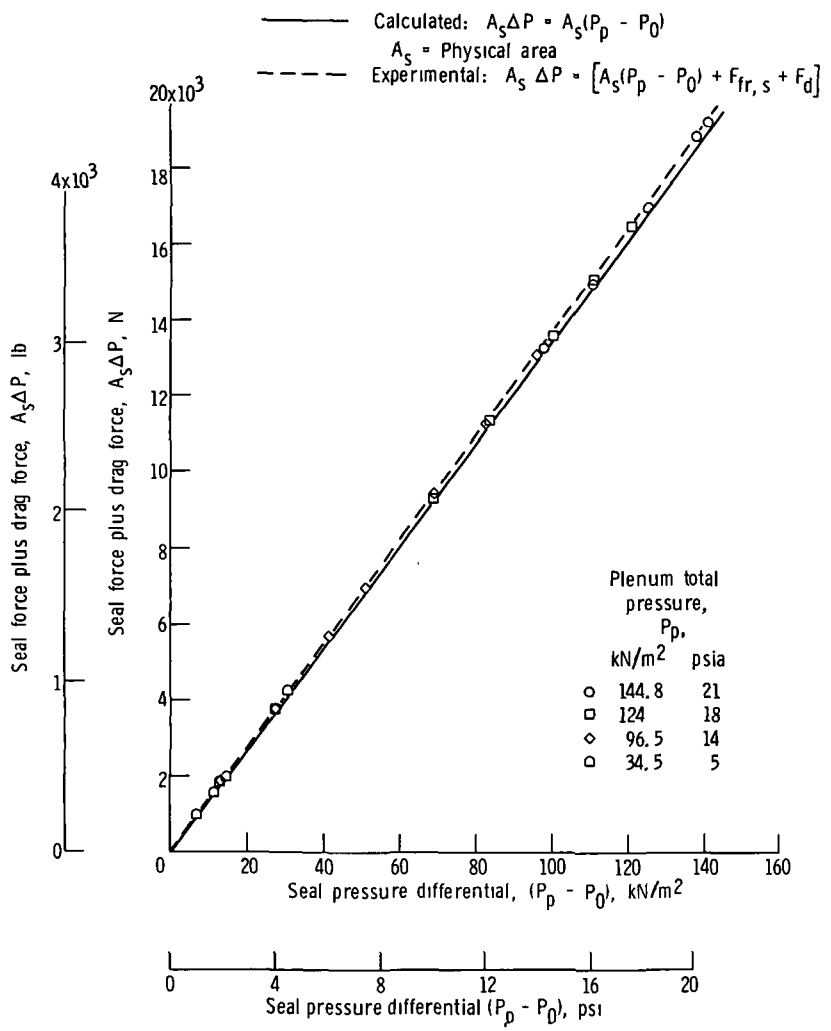

Figure 10. - Combined seal force and drag force as function of pressure differential.

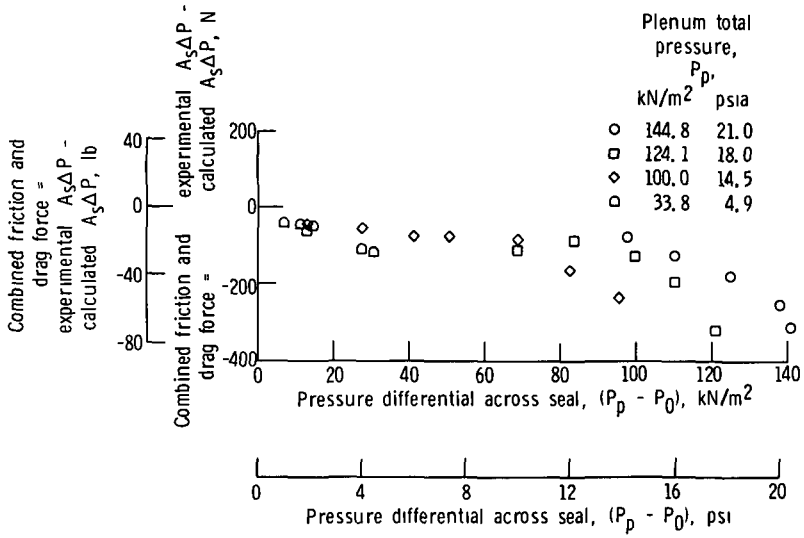

Figure 11. - Combined friction force and drag force as function of pressure differential across seal.

most straight line which passes through the origin. This indicates generally good seal design and linearity of the system. Also shown on this figure is the calculated $A_s \Delta P$ based on the physical seal area (A_s) and the measured $\Delta P(P_p - P_0)$. Figure 11 shows the difference between the measured and calculated seal force (friction) and base drag force term plotted against $(P_p - P_0)$. This term is obtained by subtracting the calculated seal force from the experimentally measured force and is an indication of the drag component included in the overall measured term.

Bellmouth Pressure Forces

The combined forces acting on the curved and varying-area surface of the bellmouth was calculated by equation (11). Figure 12 shows the combined bellmouth inlet forces divided by the plenum pressure as a function of the corrected airflow.

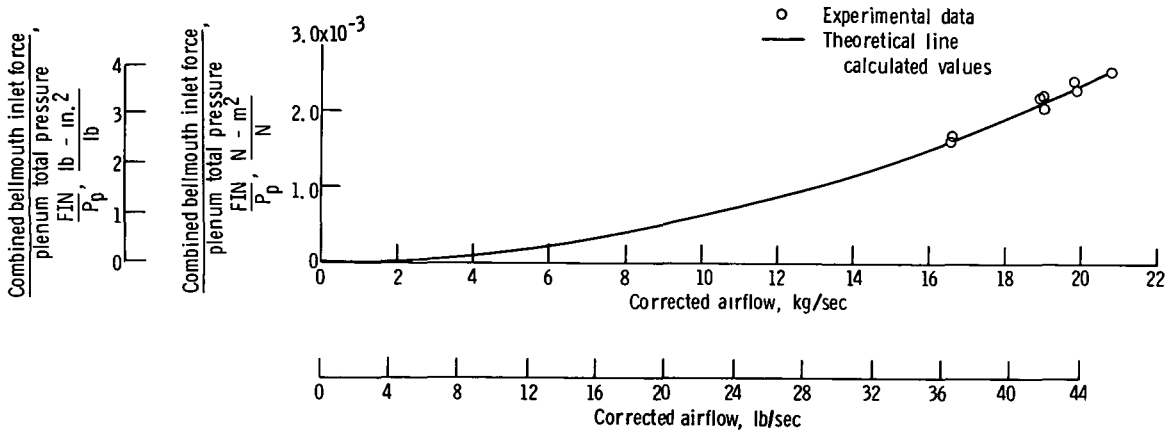

Figure 12. - Theoretical and experimental combined inlet force over plenum total pressure as function of corrected inlet airflow.

Gross Thrust

The sum of the measured thrust, the seal force plus drag force, and the combined bellmouth inlet force determines the gross thrust produced. A typical plot of gross thrust against exhaust nozzle pressure ratio, P_7/P_0, with inlet pressure constant for cold flow is presented in figure 13.

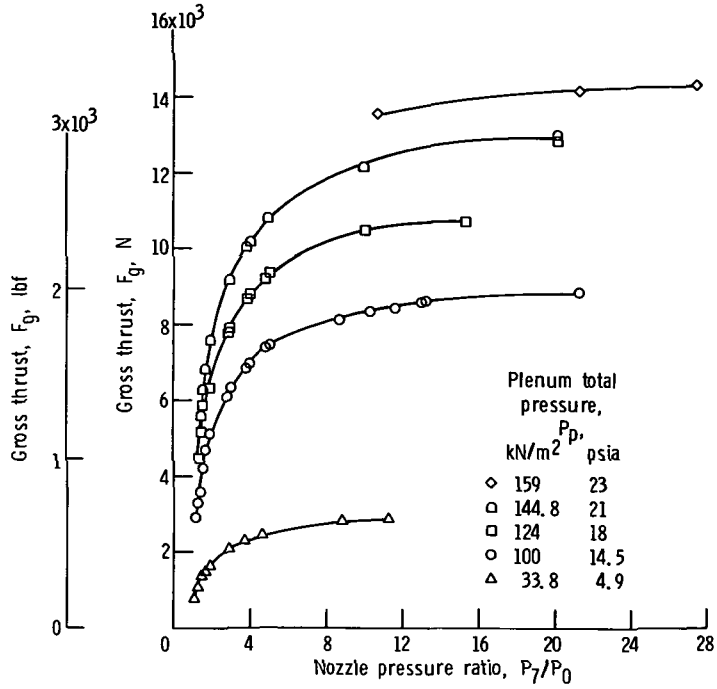

Figure 13. - Gross thrust (from cold flow data) as function of nozzle pressure ratio. Nozzle throat area, 694 square centimeters (107.5 in.^{2}). Inlet pressure held constant.

Isentropic Thrust Coefficient

The ratio of gross thrust to the maximum thrust produced under isentropic conditions is defined as the isentropic thrust coefficient and is a measure of the nozzle thrust efficiency. These parameters for the range of nozzle pressure ratios tested are presented in figure 14.

Actual Gross Thrust Coefficient

The commonly defined thrust coefficient, $C_{F,id}$ in the ideal thrust equation

$$F_{id} = C_{F,id} P_7 A_8 C_{D,n} \tag{20}$$

is a straight line with a slope of A_9/A_8 when plotted as a function of P_0/P_7. The calculated gross thrust can define a similar parameter called the actual gross thrust coefficient. A typical comparison of these two coefficients is shown in figure 15. At low values of P_0/P_7, the C_F values cluster quite close to the slope line of the ideal case

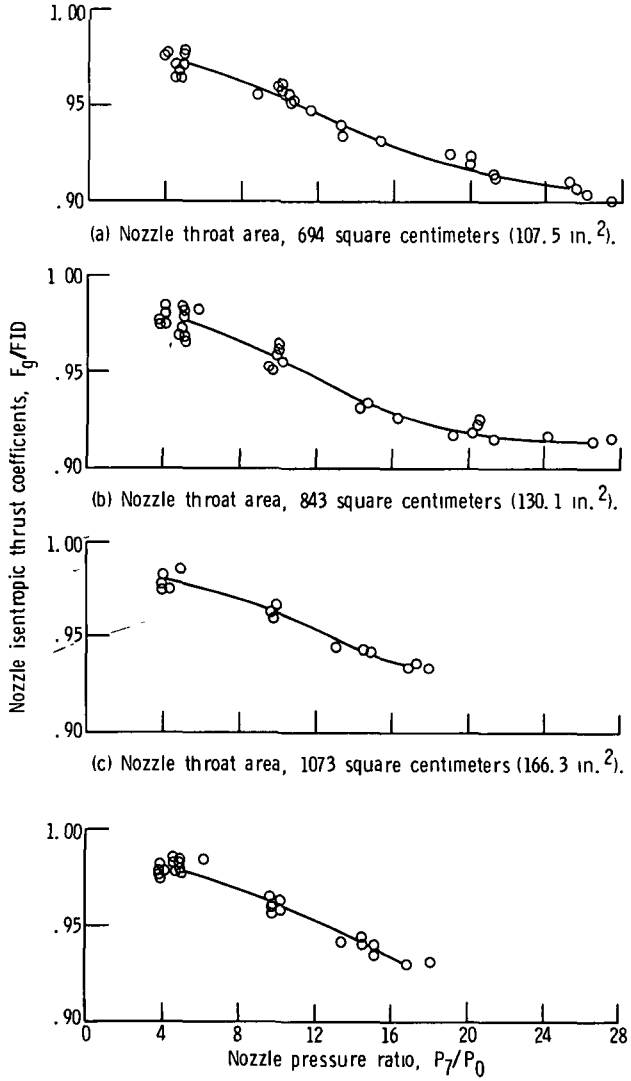

(a) Nozzle throat area, 694 square centimeters (107.5 in.^{2}).

(b) Nozzle throat area, 843 square centimeters (130.1 in.^{2}).

(c) Nozzle throat area, 1073 square centimeters (166.3 in.^{2}).

(d) Nozzle throat area, 1186 square centimeters (183.8 in.^{2}).

Figure 14. - Nozzle isentropic thrust coefficients for cold-flow data as function of nozzle pressure ratio.

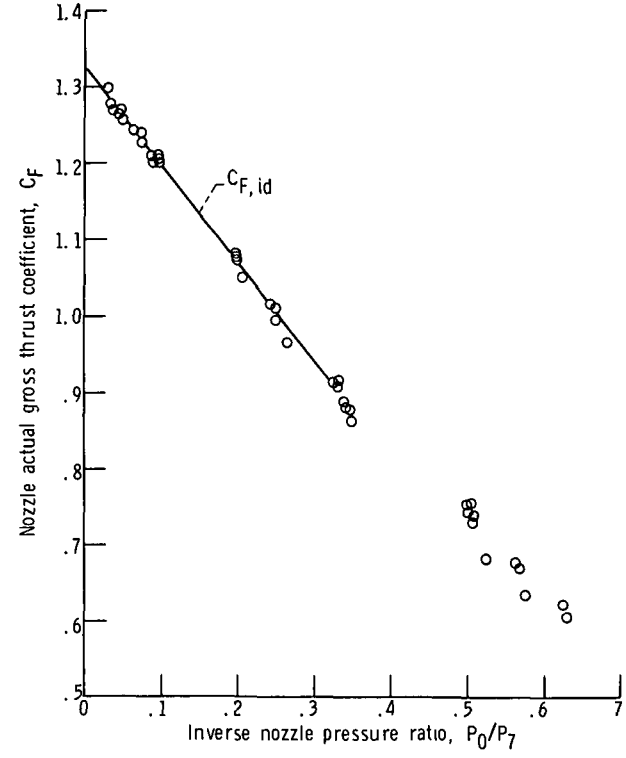

Figure 15. - Nozzle actual gross thrust coefficient as function of inverse nozzle pressure ratio for cold-flow tests showing effects of nozzle flow separation at inverse nozzle pressure ratio of ≈0.35. Nozzle throat area, 694 square centimeters (107.5 in.^{2})

and this serves as a check that the nozzle is flowing full. Deviation of the gross thrust coefficient values from the ideal slope line where $P_0/P_7 \approx 0.35$ is an indication that the exhaust gas is separated from the wall and the nozzle is no longer flowing full. This detached flow can be highly asymmetrical as well as unsteady. Data beyond this point are probably not applicable in a steady-state performance evaluation program.

Hot-Gas Flow Tests

In the hot-gas test runs, a J85 turbojet engine was installed as a gas generator, and tests were run with exhaust gas temperatures up to 1944 K (3500° F). For the 694 and 843 square centimeters (107.5 and 130.7 in.^{2}) nozzles, the temperatures at the nozzle inlet were measured with temperature rakes. For the 1073 and 1186 square centimeters (166.3 and 183.8 in.^{2}) nozzles, the temperatures were calculated using choked flow relations due to difficulty of measuring high temperatures resulting from afterburner operation.

The gross thrust was again the sum of the measured thrust, the combined bellmouth inlet force, and the seal force plus drag force. Using gross thrust values, the isentropic thrust coefficients were calculated and are presented in figure 16 for each of the nozzles.

Actual gross thrust coefficients were calculated and a typical result is presented in figure 17 for the 694-square-centimeter (107.5-in.^{2}) nozzle. As in the case of the cold-flow data, the hot-gas data follows the slope of the ideal case at low values of P_0/P_7. Deviation of the gross thrust coefficient values from the ideal slope at values of $P_0/P_7 \approx 0.35$ is again an indication of nozzle flow separation.

Comparison of Hot-Gas and Cold-Flow Results

One of the prime purposes of these tests was to determine how accurately gross thrust could be evaluated for this turbojet engine and to determine if the method used for measuring thrust in these tests could also be used for other engine and nozzle tests.

Experimental nozzle tests reported in references 9 and 10 showed that at a higher nozzle inlet temperature, the nozzle flow coefficient value was less than the value determined from the cold flow data. Because of these results an attempt was made to calculate hot-gas flow coefficients for the fixed-area nozzles from the hot-gas data. Figure 18 presents a typical curve of hot-gas flow coefficients as a function of nozzle pressure ratio for the 694-square-centimeter (107.5-in.^{2}) nozzle. These flow coefficients were used in determining the thrust coefficients for the four nozzles for the hot-

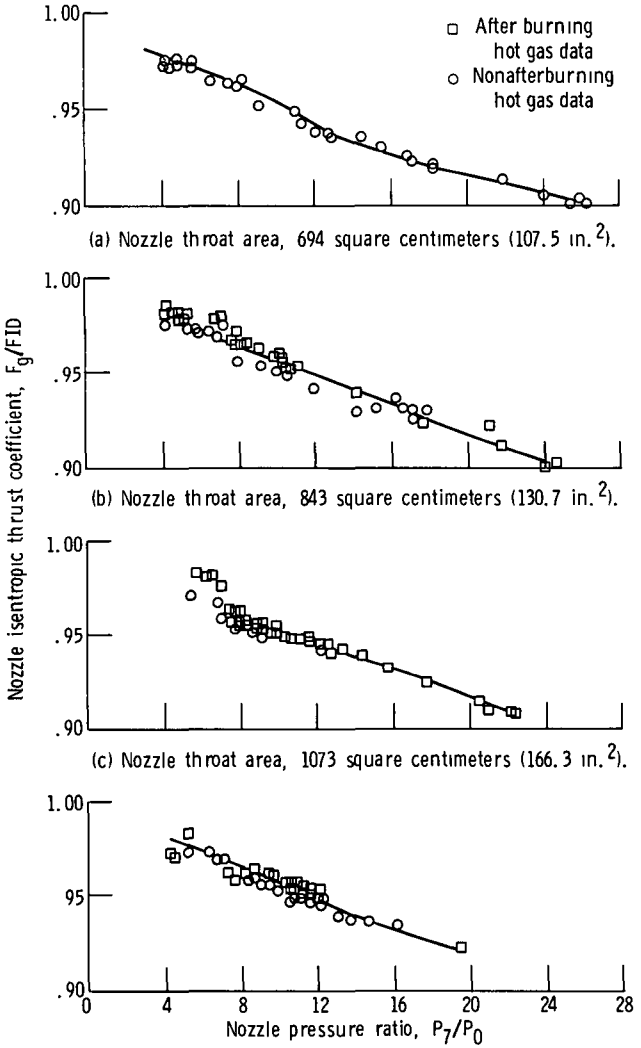

(a) Nozzle throat area, 694 square centimeters (107.5 in.^{2}).

(b) Nozzle throat area, 843 square centimeters (130.7 in.^{2}).

(c) Nozzle throat area, 1073 square centimeters (166.3 in.^{2}).

(d) Nozzle throat area, 1186 square centimeters (183.8 in.^{2}).

Figure 16. - Nozzle isentropic thrust coefficients for hot-gas flow with exhaust gas temperatures up to 1944 K, 3500° R as function of nozzle pressure ratio.

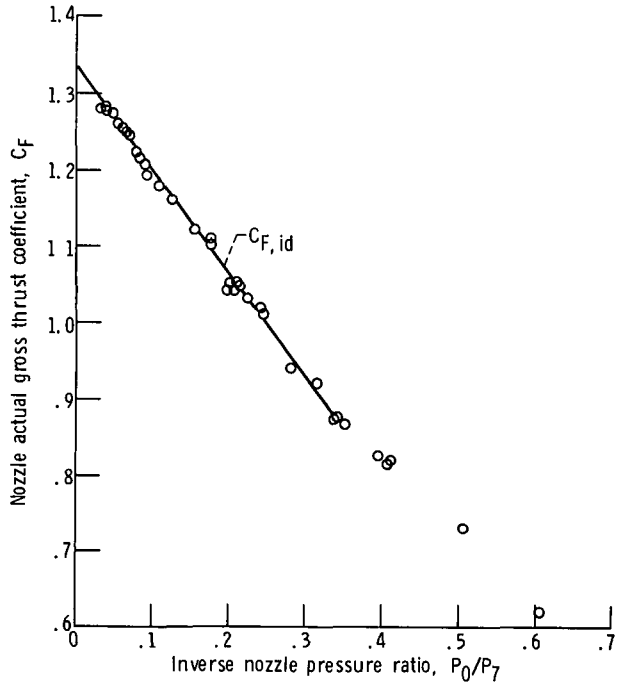

Figure 17. - Nozzle actual gross thrust coefficient as function of inverse nozzle pressure ratio for hot-gas tests showing effects of nozzle flow separation at inverse nozzle flow separation of inverse nozzle pressure ratio of ≈ 0.35. Nozzle throat area, 694 square centimeters (107.5 in.^{2}).

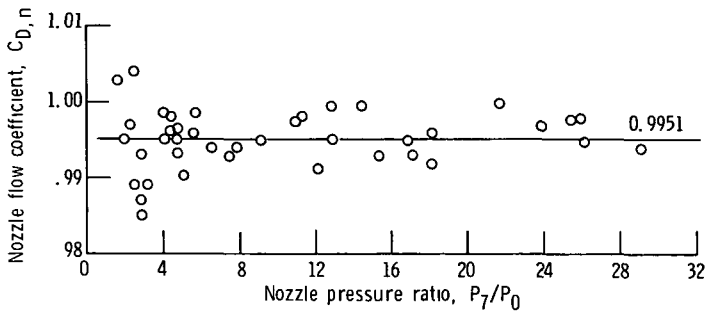

Figure 18. - Nozzle flow coefficients for 694-square centimeters (107.5-in.^{2}) nozzle from hot-gas data as function of nozzle pressure ratio.

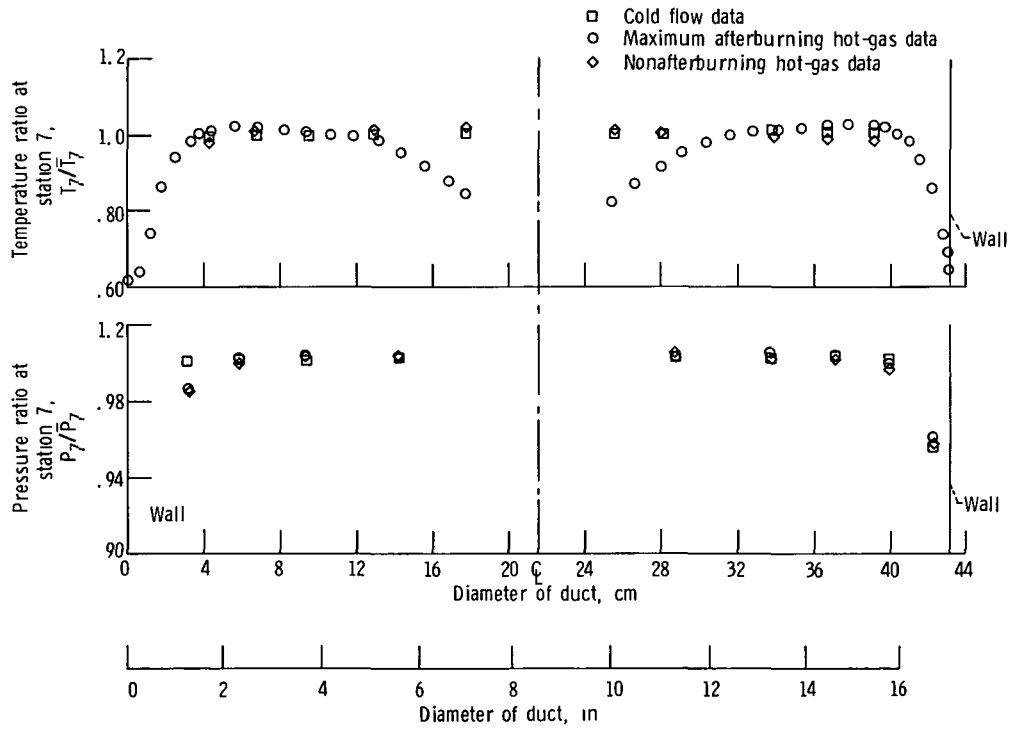

Figure 19. - Temperature ratios and total pressure ratios at station 7 as function of location at station 7. Temperatures measured with water-cooled traversing probe for afterburner operation.

gas tests. Also, figure 19 shows that the temperature profile at the nozzle inlet for hot-gas flow up to 1944 K (3500° R is quite different from the temperature profile for the cold-flow tests with ambient temperature at the nozzle inlet. The total pressure profiles at the nozzle inlet for hot-gas and cold-flow operation are presented in figure 19.

The isentropic thrust coefficients for the hot-gas and cold-flow tests as a function of nozzle pressure ratio are presented in figure 20. There is favorable agreement between these values for the hot-gas and for cold-flow data. For all the nozzles on the average, the hot-gas coefficients were within ±0.59 percent of the cold-flow base-line data.

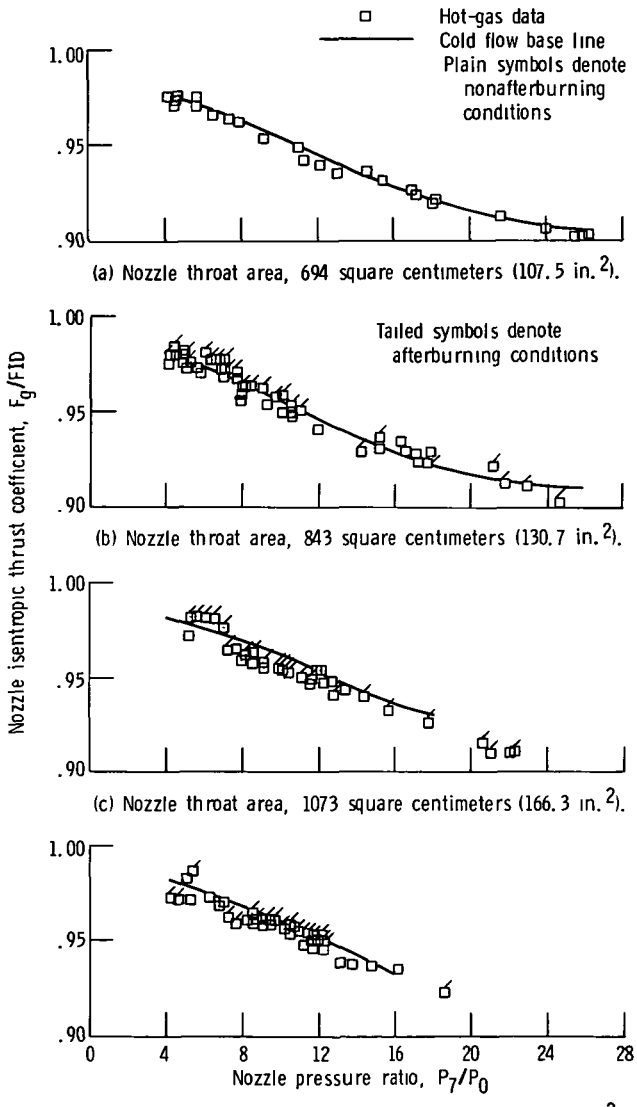

(a) Nozzle throat area, 694 square centimeters (107.5 in.^{2}).

(b) Nozzle throat area, 843 square centimeters (130.7 in.^{2}).

(c) Nozzle throat area, 1073 square centimeters (166.3 in.^{2}).

(d) Nozzle throat area, 1186 square centimeters (183.8 in.^{2}).

Figure 20. - Comparison of nozzle isentropic thrust coefficients for hot-gas flow and cold flow as function of nozzle pressure ratio

SUMMARY OF RESULTS

The cold-flow tests and the hot-gas tests conducted in this program have yielded the following principle conclusions:

1. In a well-designed test setup with an accurately calibrated thrust measuring system, gross thrust can be determined within 0.6 percent of the load cell full-scale reading for both hot-gas and cold-flow operation based on a probable error analysis.

2. A direct comparison of the nozzle isentropic thrust coefficients for both the hot-gas and cold-flow tests using the cold-flow data as a base line showed that agreement between these coefficients was on the average within ±0.59 percent for the four nozzles. The results indicate that the method used to determine gross thrust for the turbojet engine in this test could also be used in a future engine and nozzle evaluation tests.

3. In the calabration of the airflow measuring station, the bellmouth flow coefficient was calculated by two different methods. In one, the free-stream total pressure outside the boundary layer at station 1 was used; in the other, the average total plenum pressure was used. The results from the two methods are within 0.07 percent of each other. It is therefore permissible to eliminate total pressure probes at the bellmouth throat (station 1) during hot-gas runs for engine testing, when uniform flow conditions are present at the bellmouth inlet. This can help improve airflow pattern into the engine by eliminating possible wakes from the instrument rakes.

4. The flow coefficient for the airflow measuring station (station 1) was 0.984 with a scattering of ±0.4 percent.

Lewis Research Center,
National Aeronautics and Space Administration,
Cleveland, Ohio, June 30, 1971,
720-03.

APPENDIX A

SYMBOLS

A	area
a	length (nozzle inlet to throat)
abs	absolute
b	length (nozzle exit to throat)
C	coefficient
D	diameter
F	thrust or force
Gc	mass flow function
g	gravitation constant
M	Mach number
mv	momentum
P	total pressure
p	static pressure
Q	stream thrust function
R	gas constant
REI	Reynolds number index $\delta/\varphi \sqrt{\theta}$
T	total temperature
t	static temperature
V	velocity
W	flow rate
z	compressibility factor
γ	ratio of specific heats
δ	ratio of total pressure to NASA standard sea-level pressure of 101 kN/m^2 (14.696 psia)
θ	ratio of total temperature to NASA standard sea-level temperature of 288 K (518.67^{o} R)
ρ	density

φ ratio of viscosity to the viscosity at NASA standard sea-level conditions

Subscripts:

a/b afterburner

bm bellmouth

D flow or discharge

d drag

exit nozzle exit, station 9

F thrust

fr friction

g gross

id ideal (one dimensional)

in inlet station of bellmouth

K annulus number

L local

m measured

n exhaust nozzle

P plenum

s seal

sl sea-level

0 altitude chamber

1 bellmouth throat

7 exhaust nozzle inlet

8 exhaust nozzle throat

9 exhaust nozzle exit

Superscripts:

— average

* critical state (M = 1)

APPENDIX B

DETERMINATION OF AIRFLOW ERROR

A calculation was made to determine the error in airflow due to assuming $\gamma = 1.4$. For the design Mach of 0.6 for the bellmouth throat and for the range of temperatures covered, the deviation was approximately +0.028 percent.

The cumulative error due to various measurement and recording errors from individual instrumentation is in table V. The error given for each individual item was supplied by the manfacturer.

TABLE V. - INDIVIDUAL AND CUMULATIVE ERRORS OF INSTRUMENTATION

[Values in percent.]

	Error	Cumulative error
Damper	0.1	0.1
Load cell	0.1	0.105
Digital counter	0.1	
Thermocouple	0.375	0.45
Oven	0.2	
Average digital error	0.15	

The probable error resulting in the airflow calculation due to instrumentation errors shown in table V can be estimated as follows:

$$W_1 = C_{d,bm} W_{1,id} = C_{d,bm} A_1 P_{1,id} \left[\frac{2g\gamma}{RT(\gamma - 1)}\right]^{1/2} \left(\frac{p_1}{P_{1,id}}\right)^{1/\gamma}$$

$$\times \left[1 - \left(\frac{p_1}{P_{1,id}}\right)^{(\gamma-1)/\gamma}\right]^{1/2} \qquad \text{(B1)}$$

Letting

$$k_1 = \left(\frac{2g}{R}\,\frac{\gamma}{\gamma - 1}\right)^{1/2}$$

$$k_2 = \frac{\gamma - 1}{\gamma} = \frac{2}{7}$$

$$k_3 = \frac{1}{\gamma} = \frac{5}{7}$$

$$W_1 = k_1 C_{d,bm} A_1 \left(P_{1,id}\right)^{k_2} \left(p_1\right)^{k_3} \left(T_1\right)^{-1/2} \left[1 - \left(\frac{p_1}{P_{1,id}}\right)^{k_2}\right]^{1/2} \tag{B2}$$

Differentiating equation (B2), then dividing by W_1 and letting $(dy/y) = (\Delta y/y)$, yield

$$\frac{\Delta W_1}{W_1} = \left(\frac{\Delta C_{d,bm}}{C_{d,bm}}\right) + \left(\frac{\Delta A_1}{A_1}\right) + \left(-\frac{1}{2}\right)\left(\frac{\Delta T_1}{T_1}\right) + \left\{k_2 \frac{1}{P_{1,id}} + \frac{1}{2}\left[1 - \left(\frac{p_1}{P_{1,id}}\right)^{k_2}\right]^{-1}\right.$$

$$\left. \times (+k_2) p_1^{(k_2)} \left(P_{1,id}\right)^{-(k_2+1)} \right\} \Delta P_{1,id} + \left\{k_3 \frac{1}{p_1} + \frac{1}{2}\left[1 - \left(\frac{p_1}{P_{1,id}}\right)^{k_2}\right]^{-1}\right.$$

$$\left. \times (-k_2) p_1^{(k_2-1)} \left(P_{1,id}\right)^{-k_2} \right\} \Delta p_1 \tag{B3}$$

$$ep^2 = \left(\frac{\Delta C_{d,bm}}{C_{d,bm}}\right)^2 + \left(\frac{\Delta A_1}{A_1}\right)^2 + \frac{1}{4}\left(\frac{\Delta T_1}{T_1}\right)^2 + \left\{ \frac{k_2}{P_{1,id}} + \frac{1}{2}\left[1 - \left(\frac{p_1}{P_{1,id}}\right)^{k_2}\right]^{-1} \right.$$

$$\left. \times k_2 p_1^{k_2} P_{1,id}^{-(k_2+1)} \right\}^2 \left(\Delta P_{1,id}\right)^2$$

$$+ \left\{ \frac{k_3}{p_1} + \frac{1}{2}\left[1 - \left(\frac{p_1}{P_{1,id}}\right)^{k_2}\right]^{-1} (-k_2) p_1^{(k_2-1)} P_{1,id}^{-k_2} \right\}^2 \left(\Delta p_1\right)^2 \qquad \text{(B4)}$$

For bellmouth airflow Mach number = 0.6, $P_{1,id}$ = 101.4 kilonewtons per square meter absolute (14.7 psia) p_1 = 79.3 kilonewtons per square meter absolute (11.5 psia)

$$\frac{p_1}{P_{1,id}} = 0.78$$

$$\frac{\Delta C_{d,bm}}{C_{d,bm}} = 0.005$$

$$\frac{\Delta p_1}{p_1} = 0.001$$

$$\frac{\Delta P_{1,id}}{P_{1,id}} = 0.001$$

$$\frac{\Delta A_1}{A_1} = 0.001 \text{ (assumed)}$$

$$\frac{\Delta T_1}{T_1} = 0.0045$$

$$\Delta P_{1,\,id} = 0.001 P_{1,\,id} = 0.1014 \text{ kN/m}^2 \text{ (0.0147 psi)}$$

$$\Delta p_1 = 0.001 P_1 = 0.0793 \text{ kN/m}^2 \text{ (0.0115 psi)}$$

Substituting these values and constants k_2 and k_3 into equation (B4) gives $(ep)^2 = (0.00610)^2$ or a probable error of 0.61 percent.

APPENDIX C

RESULTANT ERROR IN GROSS THRUST MEASUREMENTS DUE TO INSTRUMENTATION ERRORS

Using equation (10), the gross thrust is

$$F_g = F_m + \left[(mv)_{in} + P_{in}A_{in} - P_pA_{in}\right] + \left[A_s(P_p - P_0) + F_{fr,s} + F_d\right]$$

Since the quantity $\left[A_s(P_p - P_0) + F_{fr,s} + F_d\right] = F_s$ is measured as one quantity (see fig. 10), it is not necessary to evaluate the errors contributed by A_s, P_p, P_0, $F_{fr,s}$, and F_d separately. Instead, the measurement error in F_s as a whole will be used.

Therefore, letting $\left[(mv)_{in} + P_{in}A_{in} - P_pA_{in}\right] = FIN$,

$$F_g = F_m + F_s + FIN$$

Substituting the definition of FIN (eq. (11)) yields

$$F_g = F_m + F_s + P_pA_{in}(Q - 1)$$

The absolute value of the error in gross thrust measurement is

$$\Delta F_g = \Delta F_m + \Delta F_s + P_p\Delta A_{in} + A_{in}\Delta P_p$$

The probable error expressed as a fraction of the gross thrust measurement is

$$\left(\frac{\Delta F_g}{F_g}\right)^2 = \frac{1}{(F_g)^2}\left[(\Delta F_m)^2 + (\Delta F_s)^2 + (\Delta P_pA_{in})^2 + (P_p\Delta A_{in})^2\right] \qquad (C1)$$

Assume $P_p = 144.8 \times 10^3$ newtons per square meter absolute (21 psia), $F_g = 22\ 240$N (5000 lb), $A_{in} = 0.6819$ square meter (1057 in.^{2}), M = 0.6, $\Delta F = \pm 22.24$N(± 5 lb), $\Delta P = 144.8$ newtons per square meter absolute (0.021 psia), and $\Delta A = 0.6819 \times 10^3$ square meter (1.057 in.^{2}). Substituting these values into equation (C1) results in

$$\left(\frac{\Delta F_g}{F_g}\right)^2 = \frac{1}{(5000)^2}\left[(5.0)^2 + (5.0)^2 + (1057 \times 0.021)^2 + (1.057 \times 21)^2\right]$$

$$\left(\frac{\Delta F_g}{F_g}\right)^2 = \frac{1}{(5000)^2} \times 1036$$

$$\left(\frac{\Delta F_g}{F_g}\right)^2 = 0.000041$$

$(ep)^2 = (0.0064)^2$ or a probable error of 0.64 percent.

REFERENCES

1. Antl, Robert J.; and Burley, Richard R.: Steady-State Airflow and Afterburning Performance Characteristics of Four J85-GE-13 Turbojet Engines. NASA TM X-1742, 1969.

2. Samanich, Nick E.; and Huntley, Sidney C.: Thrust and Pumping Characteristics of Cylindrical Ejectors Using Afterburning Turbojet Gas Generator. NASA TM X-52565, 1969.

3. Mansour, Ali H.; and Burley, Richard R.: Internal Thrust and Pumping Performance of an Auxiliary Inlet Ejector Nozzle with Clamshell Thrust Reserver. NASA TM X-52621, 1969.

4. Huntley, Sidney C.; and Samanich, Nick E.: Performance of a 10° Conical Plug Nozzle Using a Turbojet Gas Generator. NASA TM X-52570, 1969.

5. Staff of Lewis Laboratory: Central Automatic Data Processing System. NACA TN 4212, 1958.

6. Gracey, William; Letko, William; and Russell, Walter R.: Wind-Tunnel Investigation of a Number of Total-Pressure Tubes at High Angles of Attack-Subsonic Speeds. NACA RM L50G19, 1950.

7. Stickney, Truman M.: Recovery and Time-Response Characteristics of Six Thermocouple Probes in Subsonic and Supersonic Flow. NACA TN 3455, 1955.

8. Kennedy, E. C.: New Mach Number Tables for Ram-Jet Flow Analysis $\gamma = 7/5$ and $\gamma = 9/7$. Rep. OAL Memo 50-1, Ordnance Aerophysics Lab., Convair, Aug. 2, 1955.

9. Greathouse, W. K.: Preliminary Investigation of Pumping and Thrust Characteristics of Several Full-Size Cooling - Air Ejectors at Several Exhaust-Gas Temperatures. NACA RM E54A18, 1954.

10. Mercer, Charles E.; Schmeer, James W.; and Lauer, Rodney F., Jr.: Performance of Several Blow-in-Door Ejector Nozzles at Subsonic and Low-Supersonic Speeds. NASA TM SX-1163, 1965.

NASA-Langley, 1971 — 1 E-6392

"The aeronautical and space activities of the United States shall be conducted so as to contribute . . . to the expansion of human knowledge of phenomena in the atmosphere and space. The Administration shall provide for the widest practicable and appropriate dissemination of information concerning its activities and the results thereof."

—NATIONAL AERONAUTICS AND SPACE ACT OF 1958

NASA SCIENTIFIC AND TECHNICAL PUBLICATIONS

TECHNICAL REPORTS: Scientific and technical information considered important, complete, and a lasting contribution to existing knowledge.

TECHNICAL NOTES: Information less broad in scope but nevertheless of importance as a contribution to existing knowledge.

TECHNICAL MEMORANDUMS: Information receiving limited distribution because of preliminary data, security classification, or other reasons.

CONTRACTOR REPORTS: Scientific and technical information generated under a NASA contract or grant and considered an important contribution to existing knowledge.

TECHNICAL TRANSLATIONS: Information published in a foreign language considered to merit NASA distribution in English.

SPECIAL PUBLICATIONS: Information derived from or of value to NASA activities. Publications include conference proceedings, monographs, data compilations, handbooks, sourcebooks, and special bibliographies.

TECHNOLOGY UTILIZATION PUBLICATIONS: Information on technology used by NASA that may be of particular interest in commercial and other non-aerospace applications. Publications include Tech Briefs, Technology Utilization Reports and Technology Surveys.

Details on the availability of these publications may be obtained from:

SCIENTIFIC AND TECHNICAL INFORMATION OFFICE

NATIONAL AERONAUTICS AND SPACE ADMINISTRATION

Washington, D.C. 20546